

Atomic structure and thermally induced transformation of the crystalline BaO/Si(100) junction

M. Kuzmin,^{1,2,*} P. Laukkanen,¹ M. P. J. Punkkinen,¹ M. Yasir,¹ M. Tuominen,¹ J. Dahl,¹
J. J. K. Lång,¹ J. Mäkelä,¹ and K. Kokko¹

¹*Department of Physics and Astronomy, University of Turku, FI-20014 Turku, Finland*

²*Ioffe Physical-Technical Institute, Russian Academy of Sciences, St. Petersburg 194021, Russian Federation*

(Received 28 July 2014; revised manuscript received 18 November 2014; published 1 December 2014)

Atomic structure of interfaces between oxide layers and semiconductors is usually challenging to probe because of its buried nature. Here, we present a synchrotron photoemission approach to unveil the interface structure of BaO/Si(100), a prototype model of crystalline-oxide/semiconductor junctions, and demonstrate that such interface outspreads over four Si atomic planes and contains five different crystal sites for Si atoms, including three Si-O bonding sites. An atomic model is suggested for this system. Heating enhances Si diffusion and oxidation, but the junction still remains crystalline at 500 °C, promising potential for integration of III-V films and Si(100).

DOI: [10.1103/PhysRevB.90.235405](https://doi.org/10.1103/PhysRevB.90.235405)

PACS number(s): 68.35.Ct, 79.60.Jv

I. INTRODUCTION

Oxide films (OF) on semiconductor crystals have attracted great interest from fundamental and technological viewpoints [1–7]. In contrast to amorphous OF, crystalline OF on semiconductors provide a well-defined platform to investigate, e.g., the atomic and electronic structure, reactivity, and electrical properties of oxide/semiconductor junctions (OSJ) at the atomic scale. Understanding these issues is essential to develop the OSJ applications in electronics, photonics, and medicine [8–13]. Moreover, it is expected that significance of the atomic-scale knowledge and control of the OSJ properties will increase even further with the development of nanoscale semiconductor-based materials.

Studying OSJ is not yet straightforward, in particular, because OF are usually insulating and interfaces are buried and thin. Meanwhile, most experimental tools can be categorized into the surface and bulk-sensitive ones; e.g., scanning tunneling microscopy (STM) probes mainly the uppermost atomic layer while traditional x-ray diffraction (XRD) surveys several atomic planes in a three-dimensional crystal. One potential approach to probe the interface layers is photoelectron spectroscopy (PES), which gives the chemically sensitive signal from the transitional region between semiconductor and OF provided that the latter is thin enough (≤ 3 nm). Using state-of-the-art synchrotron radiation (SR) facilities allows the tuning of probing depth and provides higher resolution and intensity than traditional photon sources.

Undoubtedly, SiO₂/Si has been the most studied OSJ [14–21] because it has enabled huge progress in microelectronics. Recently, SiO₂ has been replaced by HfO₂ in fast microprocessors, but the HfO₂/Si interface still contains SiO_x. SiO₂/Si is known to consist of three intermediate suboxides with three oxidation states (Si⁺¹, Si⁺², and Si⁺³) and respective bonding configurations via which the electronic band gap and dielectric constant develop towards SiO₂. However, there is still room for improvement in the atomic-level understanding of these junctions because SiO₂ and HfO₂ are amorphous.

Crystalline BaO/Si(100) is perhaps the simplest model system to elucidate various phenomena at OSJ [2,5–7]. To that end, understanding the atomic structure of BaO/Si(100) and its stability is a prerequisite. BaO has a dielectric constant of 34 [22], a band gap of 3.9–5.0 eV [2,23–25], and a NaCl-type lattice structure, which is only 1.6% mismatched with Si(100). SR-XRD and density functional theory have shown that the BaO/Si(100) interface has a (1×2) superstructure [5]. This periodicity derives from a structure induced by ½ monolayer (ML) of Sr atoms on Si(100) [(1×2)-Sr hereafter], which is a starting surface for the oxide growth [4,26]. The first atomic model of BaO/Sr/Si(100) (BaO/Si for clarity) is basically similar to that of (1×2)-Sr except that 1 ML of O atoms is added and each topmost layer Si atom has a bond to one O atom [5]. Thus, a single bonding site is suggested for the top-layer Si atoms at BaO/Si. However, the XRD data indicates a significantly rumpled structure, including four Si and two BaO layers adjacent to the interface [5]. Another open issue is the stability of BaO/Si during heating because the junction is grown at unusually low temperatures (23–120 °C).

Here, we reinvestigate the interface structure of BaO/Si and examine its stability, the knowledge required for understanding the fundamental aspects of OSJ, by using high-resolution SR-PES, in particular, the analysis of Si 2*p* line shape and core-level shifts (CLS), which provide a signature of atomic bonding sites and are extremely sensitive to the atomic arrangement, composition, thickness, and reactivity of BaO/Si. The results demonstrate that the interface consists of five different Si crystal sites, of which three arise from different Si-O environments, and that postheating induces dramatic changes in the interface structure via enhanced Si oxidation, keeping the junction crystalline.

II. EXPERIMENTAL

The experiments were carried out in two separate ultrahigh vacuum (UHV) systems. The SR-PES measurements were made on beamline I4 at the MAX-lab (Sweden). The photoelectron spectra were acquired at room temperature (RT), with an instrumental resolution better than 65 meV. In core-level measurements, the photon energy (*hν*) was optimized to enhance the Si 2*p* signal from the interfaces. The binding

*Corresponding author: m.kuzmin@mail.ioffe.ru

energy (BE) was aligned to the Fermi-level position measured from a reference Ta sample in contact with the Si sample. The STM measurements were performed in the UHV system (Omicron) with a base pressure below 1×10^{-10} Torr at the University of Turku. The images were taken with tungsten tips in the constant-current mode at RT. The WSxM package [27] was partially used for processing the STM data.

The Si(100) surfaces (n type, $1 \Omega\text{-cm}$) were cleaned by rapid flashings at 1225°C in UHV ($\sim 10^{-11} - 10^{-10}$ Torr) and verified by low-energy electron diffraction (LEED) and Si $2p$ and valence-band (VB) measurements. Sample heating was performed by a direct current. The temperature was measured by infrared pyrometers. Alkaline-earth metals (Ba and Sr) were deposited from homemade tungsten-filament evaporators. One ML is referred to as the atomic density on Si(100) (i.e., 6.78×10^{14} atoms/cm 2).

III. RESULTS AND DISCUSSION

Clean Si(100) is unsuitable for growing BaO because barium further promotes the Si oxidation [28]. To overcome this problem, the Si dangling bonds should be eliminated prior to growth [4,26]. In this paper, 0.5 ML of Sr atoms were deposited on Si at RT, followed by annealing at $530\text{--}600^\circ\text{C}$, leading to $(1 \times 2)\text{-Sr}$. Figure 1(a) presents a LEED pattern from such a structure. Electropositive Sr donates electrons to the surface, symmetrizing the Si dimers: in VB spectra shown in Fig. 1(b), a sharp peak, which is marked by an arrow and is due to the dangling bond state of the Si(100) dimer-up atom [29], disappears after the Sr adsorption.

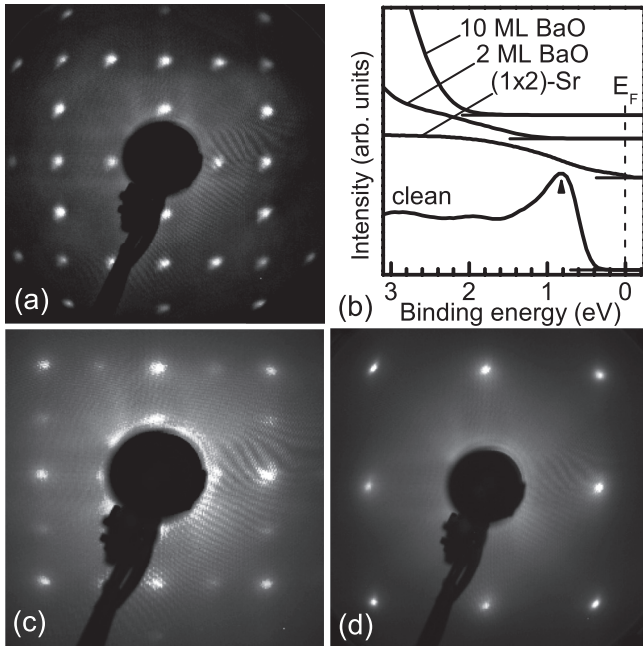


FIG. 1. (a) LEED pattern for the $(1 \times 2)\text{-Sr}$. The electron energy is 129 eV. (b) VB spectra of clean Si(100), $(1 \times 2)\text{-Sr}$, and BaO/Si grown at RT with 2 and 10 ML of Ba. The photon energy is 21 eV. (c) and (d) LEED patterns for the BaO/Si at RT and 2 and 25 ML of Ba, respectively. The electron energies are (c) 137 eV and (d) 83 eV.

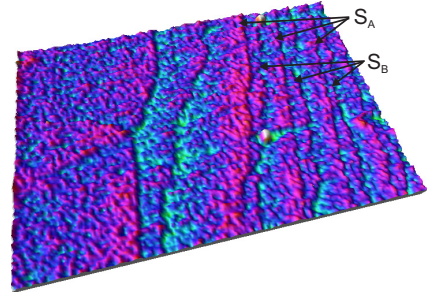


FIG. 2. (Color online) Three-dimensional STM image of BaO/Si(100) grown at 10 ML of Ba at RT. The sample bias voltage is 2.5 V, and the tunneling current is 0.25 nA. The scanning area is $1000 \times 680 \text{ nm}^2$. S_A and S_B steps are shown by arrows.

Crystalline BaO films were grown by deposition of Ba atoms on the $(1 \times 2)\text{-Sr}$ in O_2 ambient at RT. The oxygen pressure was 8×10^{-8} Torr with a Ba flux of $\sim 0.65\text{--}0.70$ ML/min. The thickness of BaO is expressed in deposited barium amounts. Low-energy electron diffraction showed that the (1×2) superstructure persists at 2 ML [Fig. 1(c)] and eventually vanishes at ~ 5 ML. Instead, a sharp (1×1) pattern became apparent [Fig. 1(d)], and it was observed up to 25 ML (the maximum Ba coverage here). It is unlikely that the (1×2) spots in Fig. 1(c) originate from bare $(1 \times 2)\text{-Sr}$ areas (i.e., holes in the BaO film) because the VB spectrum of 2-ML BaO/Si does not show any emission near the Fermi edge [Fig. 1(b)], which would be a signature of $(1 \times 2)\text{-Sr}$. Hence, the (1×2) symmetry is characteristic of the interface structure, as the previous model suggests. For the bulklike film (10 ML), the VB offset between BaO and Si is found to be 1.9 ± 0.2 eV in Fig. 1(b), in agreement with Ref. [2]. This indicates the conduction band offset of $0.9\text{--}2.0$ eV, depending on the BaO band gap ($3.9\text{--}5.0$ eV). A three-dimensional STM image of the 10-ML BaO film is presented in Fig. 2. It is seen that the top of this film is very smooth and exhibits the well-defined terrace-step structure. There are two types of steps, more straight (labeled S_A) and more rough (labeled S_B), which resemble the original steps on the clean Si(100) surface (e.g., see Ref. [30]). The presence of such steps on top of 10-ML BaO supports well the crystalline nature of the grown film, in agreement with LEED.

As $(1 \times 2)\text{-Sr}$ and Si suboxides can be building blocks of BaO/Si, we first acquired Si $2p$ spectra of $(1 \times 2)\text{-Sr}$ and $\text{SiO}_2/\text{Si}(100)$. These spectra are presented in Fig. 3. They were analyzed by using a linear combination of spin-orbit split Voigt doublets and several physically reasonable constraints. In particular, the spin-orbit splitting (608 meV), Lorentzian width (85 meV), and branching ratio (0.50 ± 0.05) were fixed for all components. The CLS and Gaussian widths (GW) were variable parameters. The experimental data are shown by circles and the fitting results by solid lines. The shadowed doublets represent the bulk (B) and surface/interface components. A predominant feature of $\text{SiO}_2/\text{Si}(100)$ is an extended structure in the $1.4\text{--}5.2$ eV BE range, which includes four CLS from Si atoms with different oxidation states ($\text{Si}^{1+} - \text{Si}^{4+}$) [15]. Their CLS and GW are presented in Table I. Comparison of component intensities at different emission angles (not shown here) indicates that the oxidation state of

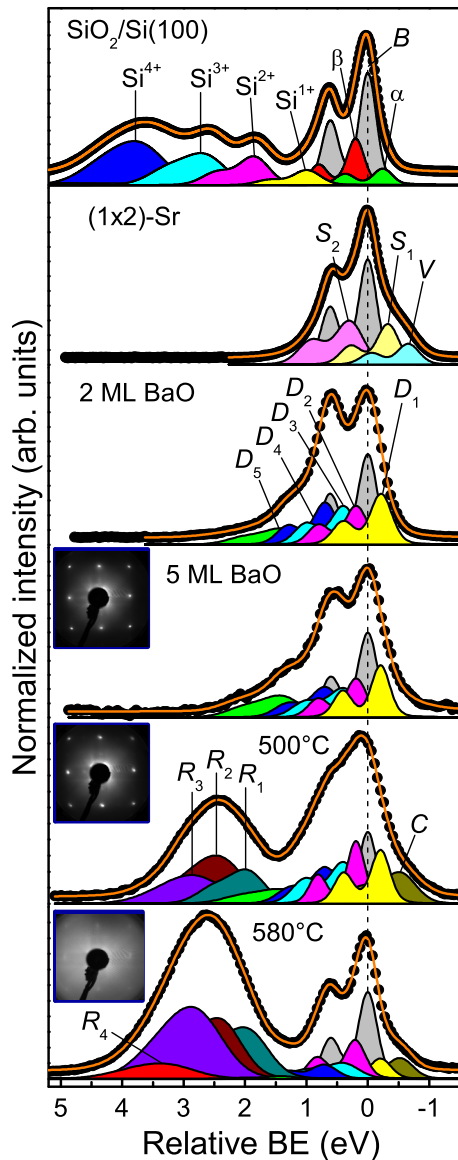


FIG. 3. (Color online) Si 2*p* spectra for SiO₂/Si(100), (1×2)-Sr, and BaO/Si measured at the photon energy of 138, 134, and 166 eV, respectively. SiO₂/Si is grown at 600 °C with the O₂ dose of 150 L. BaO/Si is produced at RT with 2 and 5 ML of Ba. The 5-ML BaO/Si is annealed at 500 and 580 °C. The spectral background is removed using Shirley's method. Each spectrum is normalized to its maximum. The bulk- and surface/interface-related components are labeled. The insets show LEED patterns for the 5-ML BaO/Si junctions at RT, 500, and 580 °C. The electron energies are 85, 83, and 86 eV, respectively.

Si atoms increases toward the surface. Also, GW increases from Si¹⁺ to Si⁴⁺.

(1×2)-Sr does not reveal any extended structure on the high BE side, however, the spectrum has a shoulder on the low BE side, contributed by surface components S₁ and V, and an additional surface component S₂ on the opposite side (Table I). The structure of (1×2)-Sr is still under debate [26,31]. Nevertheless, taking into account the attenuation model [32], CLS, and intensity ratios of the above components, we assume that S₁ and V originate from the first-layer Si atoms and the S₂ from the Si atoms in the second and partly third layers of (1×2)-Sr.

Si 2*p* spectra of BaO/Si at 2 and 5 ML are also shown in Fig. 3. They indicate that the interface structure is not affected significantly by the film thickness. Both spectra include the same interface-induced components D₁–D₅ (Table I) with similar GW and intensity ratios. The extended high BE structure of SiO₂/Si(100) is missing in these spectra, indicating a lack of Si atoms with high oxidation states at BaO/Si.

Based on the attenuation model [32], experimental conditions, and intensity ratios, we find that the amount of interface-affected Si atoms at BaO/Si (i.e., origins of D₁–D₅) is ~4 ML. Similarly, the amount of Si atoms at (1×2)-Sr is ~2.5 ML. This infers that the BaO/Si interface is not atomically abrupt and that its Si structure is significantly rearranged as compared to that of (1×2)-Sr. Because D₁ and D₂ have relatively small CLS and GW, the respective Si atoms do not interact directly with oxygen and can be located at the bottom of the BaO/Si interface adjacent to the Si bulk. D₃–D₅ have larger CLS and GW; therefore, they arise from Si atoms bonded directly to oxygen atoms. Such assignments are consistent with those for other semiconductors like III-Vs with surface oxide phases [9,33,34] as well as the rumpling of four Si layers at BaO/Si (Ref. [5]). In the BaO/Si model, however, there is only a single Si site having a bond to O [5]; therefore, this model cannot explain the present Si 2*p* data.

A more detailed interpretation can be made on the basis of CLS predicted for various Sr(Ba)-Si-O bonding configurations. Figure 4 schematically illustrates different bonding

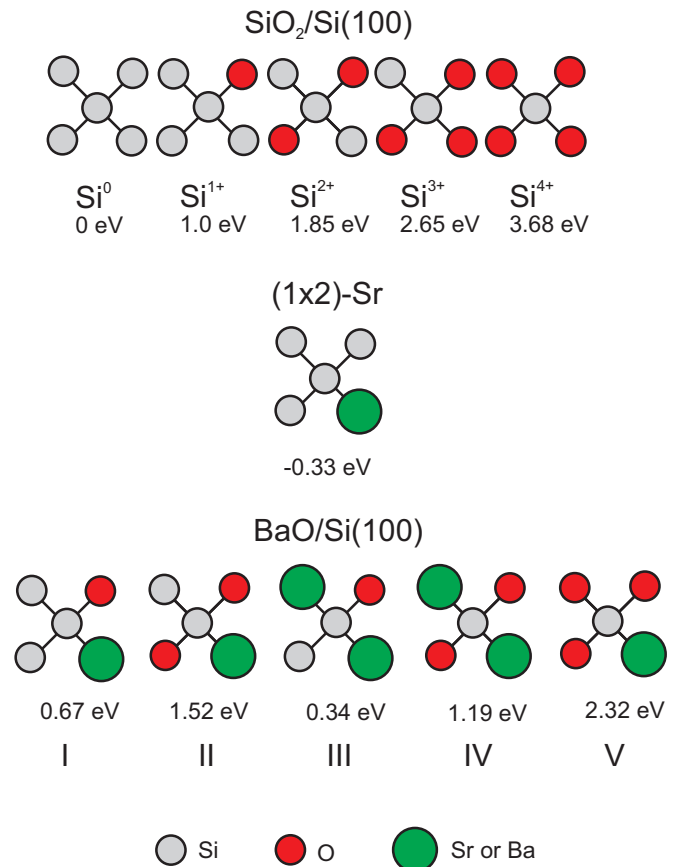


FIG. 4. (Color online) Bonding configurations and Si 2*p* CLS for SiO₂/Si(100), (1×2)-Sr, and BaO/Si. Possible metal-Si-O configurations are labeled I, II, III, IV, and V.

TABLE I. CLS and GW of Si 2*p* components for SiO₂/Si(100), (1×2)-Sr, and BaO/Si. The values are given in eV. The BaO/Si junctions grown at RT have the Ba amounts of 2 and 5 ML. The 5-ML BaO/Si was heated at 500 and 580 °C.

SiO ₂ /Si(100)										
	<i>B</i>	<i>α</i>	<i>B</i>	Si ¹⁺	Si ²⁺	Si ³⁺	Si ⁴⁺			
CLS	0	−0.25	0.20	0.99	1.85	2.65	3.68			
[GW]	[0.29]	[0.32]	[0.30]	[0.48]	[0.53]	[0.72]	[0.90]			
(1×2)-Sr										
	<i>B</i>			<i>V</i>	<i>S</i> ₁		<i>S</i> ₂			
CLS	0			−0.66	−0.33		0.30			
[GW]	[0.30]			[0.37]	[0.37]		[0.47]			
BaO/Si at RT										
	<i>B</i>	<i>D</i> ₁	<i>D</i> ₂	<i>D</i> ₃	<i>D</i> ₄	<i>D</i> ₅				
CLS	0	−0.21	0.19	0.40	0.70	1.39				
[GW]	[0.30]	[0.31]	[0.31]	[0.49]	[0.52]	[0.63]				
BaO/Si at 500 °C										
	<i>B</i>	<i>C</i>	<i>D</i> ₁	<i>D</i> ₂	<i>D</i> ₃	<i>D</i> ₄	<i>D</i> ₅	<i>R</i> ₁	<i>R</i> ₂	<i>R</i> ₃
CLS	0	−0.53	−0.21	0.19	0.40	0.70	1.39	1.95	2.38	2.77
[GW]	[0.30]	[0.48]	[0.34]	[0.34]	[0.52]	[0.52]	[0.62]	[0.64]	[0.67]	[0.90]
BaO/Si at 580 °C										
	<i>B</i>	<i>C</i>	<i>D</i> ₁	<i>D</i> ₂	<i>D</i> ₃	<i>D</i> ₄	<i>D</i> ₅	<i>R</i> ₁	<i>R</i> ₂	<i>R</i> ₄
CLS	0	−0.53	−0.21	0.19	0.40	0.70	1.39	1.95	2.38	2.77
[GW]	[0.30]	[0.48]	[0.34]	[0.34]	[0.52]	[0.52]	[0.62]	[0.64]	[0.67]	[1.0]

configurations and respective Si 2*p* CLS for different surfaces and interfaces. The SiO₂/Si(100) includes four Si oxidation states (Si¹⁺, Si²⁺, Si³⁺, and Si⁴⁺), in addition to oxygen-free Si bonding configuration (Si⁰). The Si⁰, Si¹⁺, Si²⁺, Si³⁺, and Si⁴⁺ have specific CLS, shown in the top panel of Fig. 4. Below, the bonding configuration of the first-layer Si atom bonded to the metal atom on the (1×2)-Sr surface is shown along with the assigned CLS. In the bottom panel, several possible bonding configurations are built up for the Si atoms at the BaO/Si. Neglecting the effects of atomic structure and final state, CLS can be predicted for these configurations. Within such a simple picture, we assume that, for instance, replacing one Si atom with a metal (Sr or Ba) atom in the Si¹⁺ state of SiO₂/Si reduces the CLS of Si¹⁺ by 0.33 eV, i.e., the resulting Sr(Ba)-Si-O configuration (labeled I in Fig. 4) has a CLS of 0.67 eV and so on. Comparison of CLS predicted for configurations I–V allows us to reject safely the configuration V (2.32 eV) for the BaO/Si because the highest BE CLS measured for the interface is 1.39 eV (*D*₅). We assume that the origin of *D*₃, of which CLS is 0.40 eV, is the configuration III (0.34 eV), the origin of *D*₄ (0.70 eV) is the configuration I (0.67 eV), and origins of *D*₅ (1.39 eV) are configurations II (1.52 eV) or/and IV (1.19 eV), while the *D*₁ and *D*₂ (−0.21 and 0.19 eV, respectively) are not due to Si atoms that have bonds to oxygen. Thus, the BaO/Si interface can include Si atoms, which have one or two bonds to O atoms and no Si atoms bonded to three and four O atoms. Namely, the Si atoms, which contribute to *D*₃ [*D*₄], are surrounded by one O and two [one] metal atoms, whereas the Si atoms, which contribute to *D*₅, are surrounded by two O and one or two metal atoms.

The above analysis allows us to reconsider the atomic structure of the BaO/Si(100) interface. We suggest a structural model assuming that (i) the initial Sr layer remains intact; (ii) O atoms occupy interstitial sites at the top of Si structure, which can be stretched by the compressively strained BaO film; and (iii) Si atoms diffuse toward the bottom of this film. The model presented in Fig. 5 includes the outermost layer Si atoms (0.5 ML) sitting at bridge sites above the second-layer Si atoms bonded to Sr [i.e., above the topmost Si layer of initial (1×2)-Sr]. Oxygen atoms are assumed to incorporate randomly between Si atoms in the upper three layers. Thus,

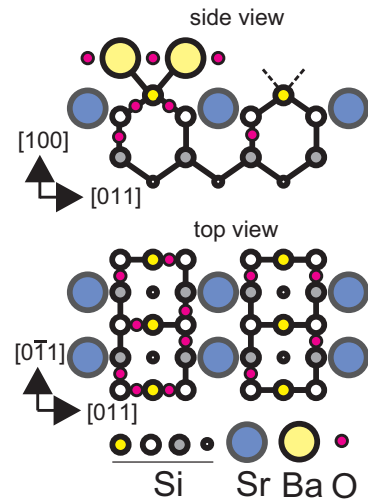


FIG. 5. (Color online) Atomic model of BaO/Si at RT. The Ba atoms are shown only in the side-view image.

the interface involves more oxygen than the previous model in Ref. [5] suggests. Finally, each uppermost Si atom has two dangling bonds that can be saturated by two Ba atoms, thereby the BaO lattice can be atomically linked with the Si(100) crystal.

The considered structure agrees well with the Si $2p$ components D_3 – D_5 arising from the Si atoms surrounded by metal and oxygen atoms in Fig. 5. Note that substitutional sites (not shown) are also possible for O atoms; however, such sites should be consistent with D_3 – D_5 as well. The D_1 and D_2 can stem from the interfacial Si atoms, which are not bonded to oxygen. Thus, the total amount of interface-affected Si atoms is about 4 ML, in agreement with the present Si $2p$ results and XRD data in Ref. [5]. Moreover, the structure in Fig. 5 reasonably explains the (1×2) periodicity of BaO/Si observed at 2 ML by LEED; indeed, the double periodicity is provided by the Sr rows, and the first BaO layers can also be distorted due to the underlying Sr rows. Finally, we anticipate that (1×2) -Sr is the best starting surface for the BaO growth because the Sr atoms (covalent radius 1.95 Å) can be readily accommodated in the Si structure of Fig. 5 with the minimum surface stress, in contrast to the other divalent metals.

To examine its stability, 5-ML BaO/Si was postheated at 500 °C for 20 min. Although no changes occurred in LEED and the film is still epitaxial, the Si $2p$ line shape shows drastic modifications upon the heating (Fig. 3). Namely, three new significantly shifted components, R_1 – R_3 (Table I), appear on the high BE side of the Si $2p$ spectrum. Five components, similar to the above D_1 – D_5 , are also found. Since R_1 – R_3 are shifted to higher BE and have larger GW than D_1 – D_5 , reasonable origins of R_1 – R_3 are Si atoms, which diffuse toward BaO and are surrounded by several oxygen atoms at the

upper silicatelike part of the interface. The amounts of Si atoms contributing to R_1 – R_3 and D_1 – D_5 are found to be ~ 1 –2 and ~ 4 ML, respectively. The corresponding regions are two constituents of the heated BaO/Si interface, suggesting the presence of Ba-silicate and oxidized (1×2) -Sr phases.

The Ba-silicate lattice should be matched well with both BaO and Si. Although various Ba-silicate compounds can form by varying the molar ratio of BaO to SiO_2 [35], only sanbornite (β - BaSi_2O_5) has a structure matched with the two lattices properly. Its lattice parameter, $b_0 = 7.69$ Å, is almost twice as large as the Si unit length (3.84 Å), i.e., the mismatch is $\leq 0.1\%$. The sanbornite structure suggests a single Si site surrounded by oxygen [35]. Si $2p$ emission, however, reveals more than one silicate-related component for the heated interface. Therefore, the environment of Si atoms in the sanbornite region can vary due to adjacent BaO and oxidized (1×2) -Sr, separating the respective Si $2p$ components (R_1 – R_3) in energy. Previously, similar CLS have been found for other Sr and Ba silicates [e.g., 2.5–2.8 eV for Sr_2SiO_4 and 3.6 eV for SrSiO_3 in Ref. [36], 1.5 eV for Sr_2SiO_4 in Ref. [37], and 2.7 eV for $(\text{Ba}_{0.8}\text{Sr}_{0.2})_2\text{SiO}_4$ in Ref. [38]].

Annealing BaO/Si at 580 °C weakens significantly the (1×1) LEED spots and causes a new Si $2p$ feature, R_4 , with the highest CLS (Fig. 3 and Table I). The total intensity of R_1 – R_3 increases, while that of D_1 – D_5 decreases by almost three times as compared to the interface at 500 °C. All these

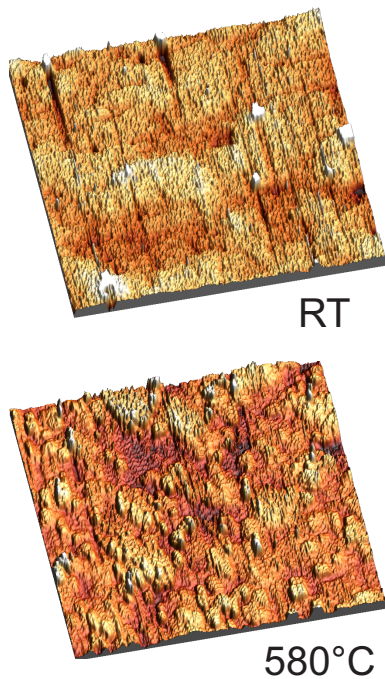


FIG. 6. (Color online) Three-dimensional STM images of 5-ML BaO/Si(100) formed at RT (top) and 580 °C (bottom). The sample bias voltage is 4.0 V, and the tunneling current is 0.1 nA. Areas: 941×941 nm² (top) and 922×922 nm² (bottom).

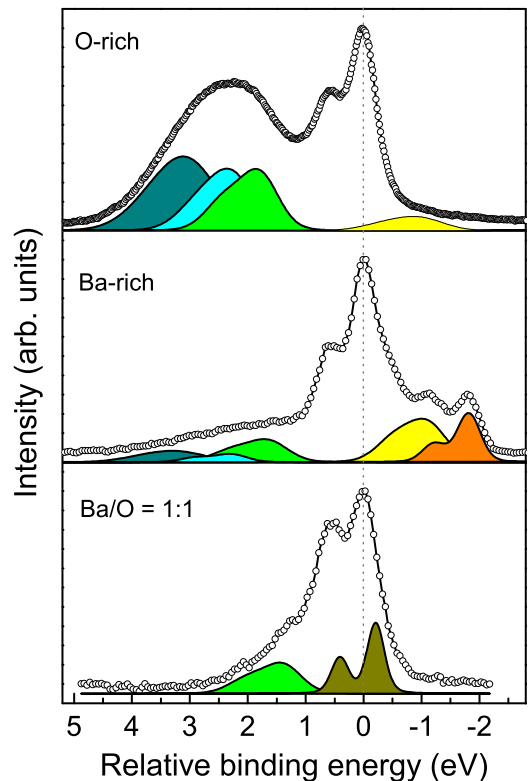


FIG. 7. (Color online) Si $2p$ spectra for the 5-ML BaO/Si(100) junction grown at RT with the optimum Ba/O ratio (bottom) and at Ba-rich (middle) and O-rich (top) conditions. The Si $2p$ components with highest and lowest BE are shown by shadowed doublets for each spectrum. The dashed line gives the position of the bulk component (0 eV). Note that Si $2p_{1/2}$ and Si $2p_{3/2}$ peaks of some doublets are not resolved because of too large GW.

changes imply enhanced Si diffusion towards the upper part of BaO/Si and thermally induced destruction of oxidized (1×2) -Sr phase. Based on the Si $2p$ data, the amounts of Si atoms in the above regions are estimated to be 3–4 and 1.0–1.5 ML, respectively. As a result, amorphous SiO_x -containing phases appear at the interface, leading to amorphization and possibly chemical transformation of the film at 580 °C. This is accompanied by the film roughening, as confirmed by STM. Figure 6 compares the surface morphology of crystalline BaO/Si(100) junction produced at RT (top panel) and amorphous BaO/Si(100) junction after heating at 580 °C (bottom panel). It is clearly seen that the thickness of the film is less uniform after the heating. These findings are not only important for understanding the crystalline OSJ but also have implications for the epitaxial growth of III-V compound semiconductor films on Si(100), which has been intensively investigated for future energy-efficient devices [6]. BaO/Si is a potential buffer layer between III-V and Si, because most III-V films are grown at 400–600 °C and BaO/Si can be kept crystalline at least at 500 °C.

The ratio of barium and oxygen is essential for the crystallinity of BaO/Si(100). In fact, the crystalline structure of BaO is favored by the high ionicity of Ba-O bonds and reduced reactivity of Si(100)(1×2)-Sr. An excess of O or Ba atoms is critically harmful and may enhance Si diffusion and oxidation and/or Ba-silicide formation. We tested the above hypothesis experimentally and grew BaO/Si junctions at RT and both Ba- and O-rich conditions, i.e., at the O_2 pressure of $(3-5)\times 10^{-8}$ and $(2-3)\times 10^{-7}$ Torr, respectively. Such junctions showed no sign of long-range order, but Si $2p$ components shifted significantly to both low and high BE sides, in contrast to the crystalline BaO/Si. Figure 7 shows Si $2p$ spectra for the crystalline BaO film grown at RT at the optimum Ba/O condition and amorphous BaO films grown at Ba- and O-rich conditions. For the crystalline junction (bottom curve), the highest and lowest BE components (indicated by shadowed doublets) are shifted by 1.39 and -0.21 eV, respectively. For the Ba-rich junction, the three highest BE components are shifted by 1.7, 2.2, and 3.1 eV; the two lowest BE components are shifted by

-1.8 and -1.1 eV. Finally, for the O-rich junction, the three highest BE components are shifted by 1.8, 2.2, and 3.0 eV; the lowest BE component is shifted by -1.0 eV. Therefore, both Ba- and O-rich amorphous junctions involve silicide and silicate phases. Thus, an excess of either species (Ba or O) stimulates an intermixing, leading to amorphous phase(s) at the interface, such as suboxides, silicates, and/or silicides.

IV. CONCLUSIONS

The atomic structure of crystalline BaO/Si(100), the prototype OSJ, has been elucidated. The findings support the presence of the interfacial (1×2) superstructure, consistent with the previous model in Ref. [5], and show that the interface consists of four affected Si planes and involves three different Si-O environments produced by the oxygen incorporation into Si. Because O incorporation into Si (i.e., Si oxidation) is the common phenomenon, the crystalline BaO/Si structure found here provides a well-defined platform to study the oxidation process and related interface defects. The heating at 500 °C enhances the Si diffusion and oxidation but keeps the crystalline interface structure. This can be provided by the sanbornitelike (BaSi_2O_5) phase, which is almost lattice matched with both BaO and Si, leading to the complex interface stack including both oxidized (1×2) -Sr and sanbornite phases. In contrast, the heating at 580 °C transforms BaO/Si to an amorphous OF via the increased Si diffusion and oxidation. The presented SR-PES-based approach is useful to elucidate the properties of various OSJ at the atomic scale.

ACKNOWLEDGMENTS

We thank the MAX-lab staff for their assistance. This paper has been supported by the European Community's Seventh Framework Programme (FP7/2007–2013) CALIPSO under Grant No. 312284, by the Finnish Academy of Science and Letters, National Doctoral Programme in Nanoscience, National Graduate School of Materials Physics, CIMO, as well as the Academy of Finland (Project No. 259213).

-
- [1] M. Hong, J. Kwo, A. R. Kortan, J. P. Mannaerts, and A. M. Sergent, *Science* **283**, 1897 (1999).
 - [2] R. A. McKee, F. J. Walker, and M. F. Chisholm, *Science* **293**, 468 (2001).
 - [3] X. Zhang, A. A. Demkov, Hao Li, X. Hu, Yi Wei, and J. Kulik, *Phys. Rev. B* **68**, 125323 (2003).
 - [4] C. J. Först, C. R. Ashman, K. Schwarz, and P. E. Blöchl, *Nature* **427**, 53 (2004).
 - [5] Y. Segal, J. W. Reiner, A. M. Kolpak, Z. Zhang, S. Ismail-Beigi, C. H. Ahn, and F. J. Walker, *Phys. Rev. Lett.* **102**, 116101 (2009).
 - [6] B. Gobaut, J. Penuelas, J. Cheng, A. Chettaoui, L. Largeau, G. Hollinger, and G. Saint-Girons, *Appl. Phys. Lett.* **97**, 201908 (2010).
 - [7] J. W. Reiner, A. M. Kolpak, Y. Segal, K. F. Garrity, S. Ismail-Beigi, C. H. Ahn, and F. J. Walker, *Adv. Mater.* **22**, 2919 (2010).
 - [8] *Materials Fundamentals of Gate Dielectrics*, edited by A. A. Demkov and A. Navrotsky (Springer, Netherlands, 2005).
 - [9] *Fundamentals of III-V Semiconductor MOSFETs*, edited by S. Oktyabrsky and P. D. Ye (Springer, New York, 2010).
 - [10] C.-L. Chang, S. K. R. S. Sankaranarayanan, D. Ruzmetov, M. H. Engelhard, E. Kaxiras, and S. Ramanathan, *Phys. Rev. B* **81**, 085406 (2010).
 - [11] *Silicon Nanocrystals: Fundamentals, Synthesis and Applications*, edited by L. Pavesi and R. Turan (Wiley-VCH, Berlin, 2010).
 - [12] P. Y. Delaunay, A. Hood, B. M. Nguyen, D. Hoffman, Y. Wei, and M. Razeghia, *Appl. Phys. Lett.* **91**, 091112 (2007).
 - [13] C. Y. Tseng, C. K. Lee, and C. T. Lee, *Prog. Photovolt. Res. Appl.* **19**, 436 (2011).
 - [14] V. V. Afanas'ev, A. Stesmans, and M. E. Twigg, *Phys. Rev. Lett.* **77**, 4206 (1996).
 - [15] J. H. Oh, H. W. Yeom, Y. Hagimoto, K. Ono, M. Oshima, N. Hirashita, M. Nywa, A. Toriumi, and A. Kakizaki, *Phys. Rev. B* **63**, 205310 (2001).

- [16] Yuhai Tu and J. Tersoff, *Phys. Rev. Lett.* **89**, 086102 (2002).
- [17] R. M. Wallace and G. D. Wilk, *Crit. Rev. Solid State* **28**, 231 (2003).
- [18] F. Giustino, P. Umari, and A. Pasquarello, *Phys. Rev. Lett.* **91**, 267601 (2003).
- [19] K. Sakamoto, H. M. Zhang, and R. I. G. Uhrberg, *Phys. Rev. B* **68**, 075302 (2003).
- [20] A. Hemeryck, A. Estève, N. Richard, M. Djafari Rouhani, and Y. J. Chabal, *Phys. Rev. B* **79**, 035317 (2009).
- [21] A. Yurtsever, M. Couillard, and D. A. Muller, *Phys. Rev. Lett.* **100**, 217402 (2008).
- [22] J. Zachariae and H. Pfnür, *Phys. Rev. B* **72**, 075410 (2005).
- [23] R. A. McKee, F. J. Walker, M. Buongiorno Nardelli, W. A. Shelton, and G. M. Stocks, *Science* **300**, 1726 (2003).
- [24] J. Robertson, *Eur. Phys. J. Appl. Phys.* **28**, 265 (2004).
- [25] T. Lv, D. Chen, and M. Huang, *J. Appl. Phys.* **100**, 086103 (2006).
- [26] J. W. Reiner, K. F. Garrity, F. J. Walker, S. Ismail-Beigi, and C. H. Ahn, *Phys. Rev. Lett.* **101**, 105503 (2008).
- [27] I. Horcas, R. Fernández, J. M. Gómez-Rodríguez, J. Colchero, J. Gómez-Herrero, and A. M. Baro, *Rev. Sci. Instrum.* **78**, 013705 (2007).
- [28] W. C. Fan and A. Ignatiev, *Phys. Rev. B* **44**, 3110 (1991).
- [29] L. S. O. Johansson, R. I. G. Uhrberg, P. Mårtensson, and G. V. Hansson, *Phys. Rev. B* **42**, 1305 (1990).
- [30] M. Kuzmin, P. Laukkanen, R. E. Perälä, R.-L. Vaara, and I. J. Väyrynen, *Surf. Sci.* **584**, 1 (2005).
- [31] J. He, G. Zhang, Q. Guo, and K. Wu, *J. Appl. Phys.* **109**, 083522 (2011).
- [32] M. P. Seah and W. A. Dench, *Surface and Interface Analysis* **1**, 2 (1979).
- [33] C. L. Hinkle, M. Milojevic, B. Brennan, A. M. Sonnet, F. S. Aguirre-Tostado, G. J. Hughes, E. M. Vogel, and R. M. Wallace, *Appl. Phys. Lett.* **94**, 162101 (2009).
- [34] J. Dahl, V. Polojärvi, J. Salmi, P. Laukkanen, and M. Guina, *Appl. Phys. Lett.* **99**, 102105 (2011).
- [35] R. C. Ropp, *Encyclopedia of the Alkaline Earth Compounds* (Elsevier, Netherlands, 2013).
- [36] M. El Kazzi, G. Delhay, C. Merckling, E. Bergignat, Y. Robach, G. Grenet, and G. Hollinger, *J. Vac. Sci. Technol. A* **25**, 1505 (2007).
- [37] Y. Liang, S. Gan, and M. Engelhard, *Appl. Phys. Lett.* **79**, 3591 (2001).
- [38] D. Müller-Sajak, S. Islam, H. Pfnür, and K. R. Hofmann, *Nanotechnology* **23**, 305202 (2012).